catalysts

MDPI

Article

Performance and Stability of Doped Ceria–Zirconia Catalyst for a Multifuel Reforming

Patrizia Frontera [1,2], Angela Malara [1], Anastasia Macario [3,*], Mariachiara Miceli [1], Lucio Bonaccorsi [1], Marta Boaro [4], Alfonsina Pappacena [4], Alessandro Trovarelli [4] and Pier Luigi Antonucci [5]

1 Department of Civil, Energy, Environment and Material Engineering, University Mediterranea of Reggio Calabria, 89124 Reggio Calabria, Italy
2 INSTM, Consorzio Interuniversitario Nazionale per la Scienza e Tecnologia dei Materiali, 50121 Firenze, Italy
3 Department of Environmental Engineering, University of Calabria, 87036 Cosenza, Italy
4 Polytechnic Department of Engineering and Architecture (DPIA), University of Udine, 33100 Udine, Italy
5 CNR, Institute of Advanced Technologies for Energy "Nicola Giordano"—ITAE, 98122 Messina, Italy
* Correspondence: author: macario@unical.it

Abstract: In the present work, the catalytic behavior of nickel-based catalysts supported on ceria/zirconia, undoped and doped with lanthanum and neodymium ($3.5Ni/Ce_{0.8}La_{0.5}Nd_{0.2}Zr_{0.13}O_{2-x}$), was investigated under different reactions: steam reforming, partial oxidation and autothermal reforming of different fuels (methane, biogas, and propane). The catalytic properties of these catalysts were evaluated at a temperature of 800 °C, under atmospheric pressure, at GSHV = 120,000 h^{-1}, using steam/carbon and oxygen/carbon ratio, respectively, of S/C = 2.5 and O/C = 0.5 and, in the case of autothermal conditions, with the addition of H_2S (100 ppm) as a contaminant. Depending on the tested fuel, ATR, SR, and POX reactions over doped and undoped catalysts showed different results. In particular, the doped catalyst, due to neodymium and lanthanum doping, better distributed nickel species on the catalyst surface, promoting a higher concentration of defect groups and oxygen vacancies. This resulted in improved catalytic performance and resistance to deactivation. Endurance catalytic test also confirmed the beneficial effect of the doped catalysts.

Keywords: reforming; hydrogen; sulfur tolerant catalysts; nickel; neodymium

Citation: Frontera, P.; Malara, A.; Macario, A.; Miceli, M.; Bonaccorsi, L.; Boaro, M.; Pappacena, A.; Trovarelli, A.; Antonucci, P.L. Performance and Stability of Doped Ceria–Zirconia Catalyst for a Multifuel Reforming. *Catalysts* **2023**, *13*, 165. https://doi.org/10.3390/catal13010165

Academic Editors: Dmitry Pashchenko and Maxim Nikitin

Received: 9 December 2022
Revised: 3 January 2023
Accepted: 6 January 2023
Published: 10 January 2023

1. Introduction

The latest IPCC report argues that stabilizing the climate will require fast actions, highlighting that the issue of climate change, due to greenhouse gas emissions, is one of the major challenges of this century that requires urgent operations [1]. Then, considerable efforts on clean energy technologies should be recommended to address this issue. The solid-oxide fuel cells (SOFCs) and solid-oxide electrolyzer cells (SOECs) are one of the most attractive renewable energy technologies that can allow this transition from a high-carbon to a low-carbon economy and finally to a zero-carbon one. Generally speaking, these devices can directly convert chemical energy from fuel into electricity [2,3] and can operate with various fuels [4]. The internal reforming has advantages in terms of energy conversion efficiency and SOFCs/SOECs system simplification reduces its cost [5]. However, the main obstacles in industrialization of multifuel SOFCs/SOECs is related to the high cost, gas contaminants, a high working temperature of ≥1000 °C and less stability due to cell degradation [6].

By the synthesis of alternative materials, the development of SOFCs/SOECs is currently focused on reducing the manufacturing costs, lowering the operating temperatures and increasing the in-service lifespan [7,8]. At the intermediate temperature (600–800 °C) the conventional anode material Ni-YSZ cermet suffers from incompatibility with hydrocarbon fuels because nickel catalyzes their decomposition, resulting in a severe deposition of carbon at the anode [9–11]. Then, catalyst deactivation and structural damage can occur

due to the carbon deposited that causes the reduction of both the cell performance and stability. These phenomena can provoke the anode volume expansion [12]. Among the different strategies to improve the catalytic performance to reduce carbon deposition in hydrocarbon fueled SOFCs/SOECs, the development of composite material is one of the most followed. Ceria–zirconia-based catalysts allow a better metal dispersion with consequent high carbon tolerance, thanks to their oxygen storage capacity. Recently, Escudero et al. have reported that a Ni-Ce-ZrO_2 system is suitable as anode material for direct reforming of biogas by solid oxide fuel cells; in fact, the incorporation of cerium in ZrO_2 improves the bulk oxygen mobility and the oxygen storage capacity of composite material, so it might mitigate the carbon deposition [13]. Moreover, the addition of the "promoters" plays a key role in the catalytic performance and stability improvement. Adding alkali metal, alkali earth metal or rare earth metals into Ni-based catalysts affects the acidic–basic properties of the catalysts and boosts the removal of deposited carbon species [13]. Osazuwa et al. in an extensive review highlighted that the lanthanide series can effectively minimize carbon formation during any form of reforming process of methane [14]. Rare-earth metal (Nd, Ce, and La) oxides were used to modify an Ni/SBA-15 catalyst, showing a stronger resistance to carbon deposition in the dry reforming of methane [15]. Perovskite-type mixed metal oxide ($CoNdO_3$) processed strong metal-support interaction, displaying high resistance to carbon formation at 750–900 °C in the CO_2 reforming process [16]. The study of the $NdCaCoO_{3.96}$ catalyst in the POX of methane has shown its superior performance: both the methane conversion and CO and H_2 selectivity increased at 850–865 °C and approached 100% selectivity and 85% methane conversion at 925 °C [16]. Recently, La and Nd ions were well incorporated in a ceria structure, in order to promote a higher abundance of defects and oxygen vacancies, resulting in a less reducible oxygen-deficient material that improves the CO oxidation activity, as a result of the weakened cerium-oxygen bonds [17].

With this background, we have investigated the performance of the nickel catalytic systems with defined ceria zirconia compositions undoped and doped with lanthanum and neodymium $Ce_{0.8}Zr_{0.2}O_2$ (CZ80) and $Ce_{0.8}Zr_{0.13}La_{0.5}Nd_{0.2}O_{2-x}$ (dpCZ80) towards the reforming reactions, namely steam reforming (SR), partial oxidation (POX) and autothermal reforming (ATR), of different fuel as well as methane, biogas and propane. Previously these system catalysts have been investigated towards dry reforming and oxidative dry reforming of methane. It was found that at 650 °C the doped catalyst led to an high conversion of both methane and carbon dioxide, with a high hydrogen selectivity and high carbon resistance [18].

Considering that the system catalysts chosen for the anode, suitable for multifuel internal reforming, should have high resistance to carbon deactivation and high resistance to sulfides eventually present in biofuels, and have also been tested for the autothermal conditions with a contamination of H_2S (100 ppm).

Conversion, selectivity, and yield are valued for every process and fuel in order to find the best operating condition to increase fuel versatility and obtain high syngas production.

2. Results and Discussion

2.1. Characterization of Catalytic Systems

XRD patterns obtained between 20° and 80° 2 theta degree are shown in Figure 1. The bare support CZ80 showed visible peaks at about 28.4°, 32.9°, 47.3° and 56.2°, which correspond respectively to the indices of (1 1 1), (2 0 0) and (3 1 1) planes of CeO_2.

The XRD profile of the support indicates that zirconia could be incorporated into the ceria lattice to form a solid solution maintaining the fluorite structure, indicating that the cubic Ce and Zr were highly homogenously distributed. According to previous studies, it was observed a shift of peaks, relative to the cubic ceria phase, to higher 2-theta ceria zirconia positions.

In the XRD profile it was observed a shift of the peaks to higher 2-theta values with respect to the undoped phases, confirming the insertion of lanthanum and neodymium into the fluorite structure. In the detail of Figure 1 the peak at 2-theta 28.6 shifts to 29.3

after the incorporation of zirconia and to 2-theta equal to 29.8 after the incorporation of neodymium and lanthanum. The profile of calcined catalysts exhibits a cubic NiO phase (JCPDS 65-7545) as indicated from the (1 1 1), (2 0 0) and (2 2 0) diffraction peaks at 2-theta 37.4, 43.4 and 62.6, respectively.

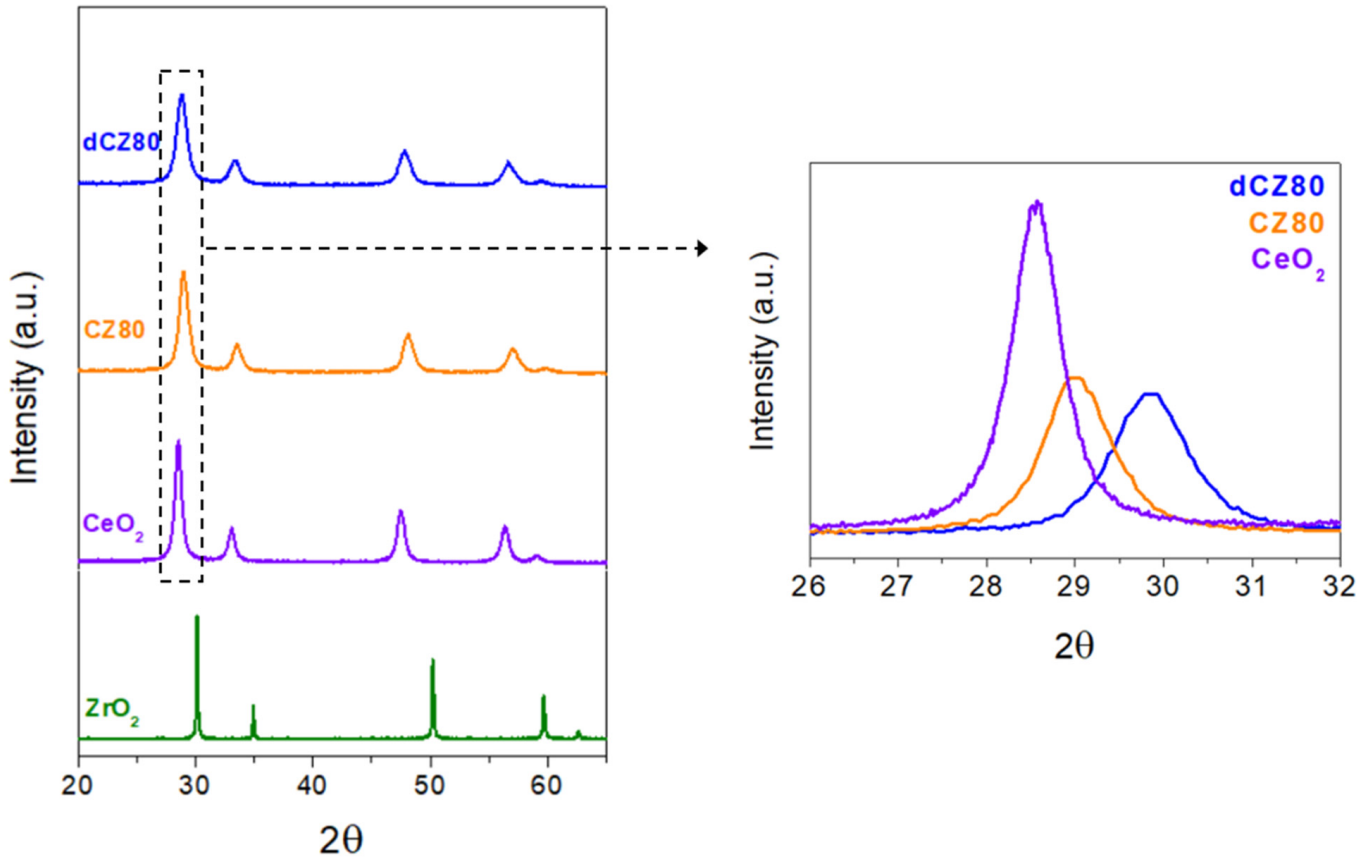

Figure 1. XRD spectra of ceria–zirconia supports, undoped and doped.

The thermal stability of the doped catalyst was investigated through the evaluation of XRD spectra recorded at increasing temperatures from 25 °C to 800 °C, indicating that the structure was retained (Figure 2). The absence of typical peaks of lanthanum and neodymium species confirmed a high thermal stability of powder without exsolution of doped elements.

Supports and catalysts were studied by SEM analysis (Figure 3). Particle distribution, heterogeneous shapes and morphologies were maintained, confirming that no significant modifications were caused after nickel impregnation and calcination treatments. In addition, EDX analysis showed the homogeneous distribution of the different elements in the catalyst (Figure 4) and the loading of the nickel metallic phase, of which the results were very close to the nominal content (3.5 ± 0.2%).

TEM images of Ni catalysts supported on undoped and doped support showed for both samples a well-defined cubic nanomorphology. Particularly, the doped sample (NidpCZ80) shows a reduced dimension with respect to the undoped sample. However, for both samples it is important to notice the complete absence of the segregation related to doping of lanthanum and neodymium, confirming the reliability of results obtained by X-ray diffraction analysis (Figure 5). Furthermore, an almost unimodal dispersion could be observed for both catalysts with slightly reduced dimensions for the doped sample. The difference can be explained considering that the incorporation of dopant ions in ceria–zirconia structure impedes the growth of the crystals, allowing the formation of smaller nanocubes.

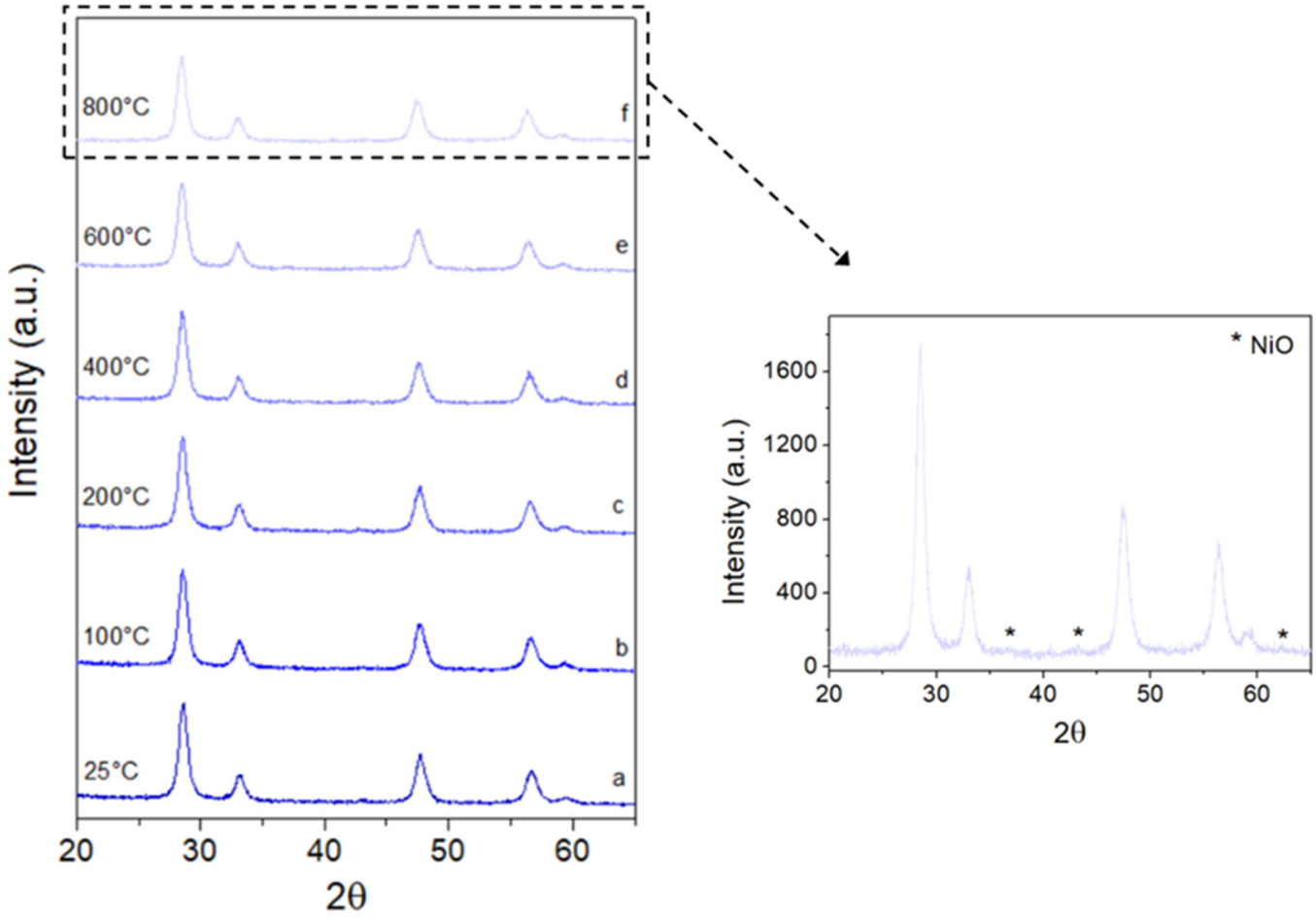

Figure 2. XRD spectra vs. temperature of doped ceria–zirconia support.

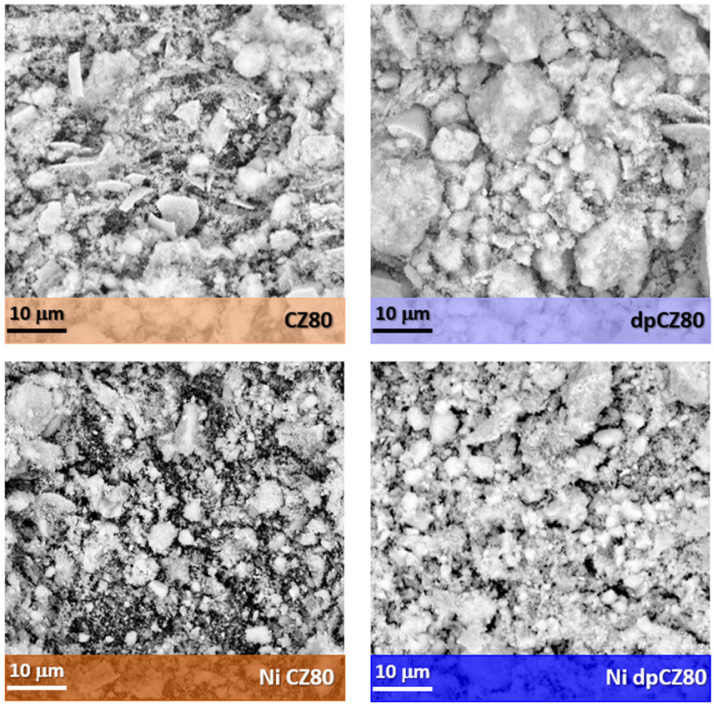

Figure 3. SEM micrographs of supports (undoped CZ80 and doped dpCZ80) and Ni supported catalysts, NiCZ80 and NidpCZ80.

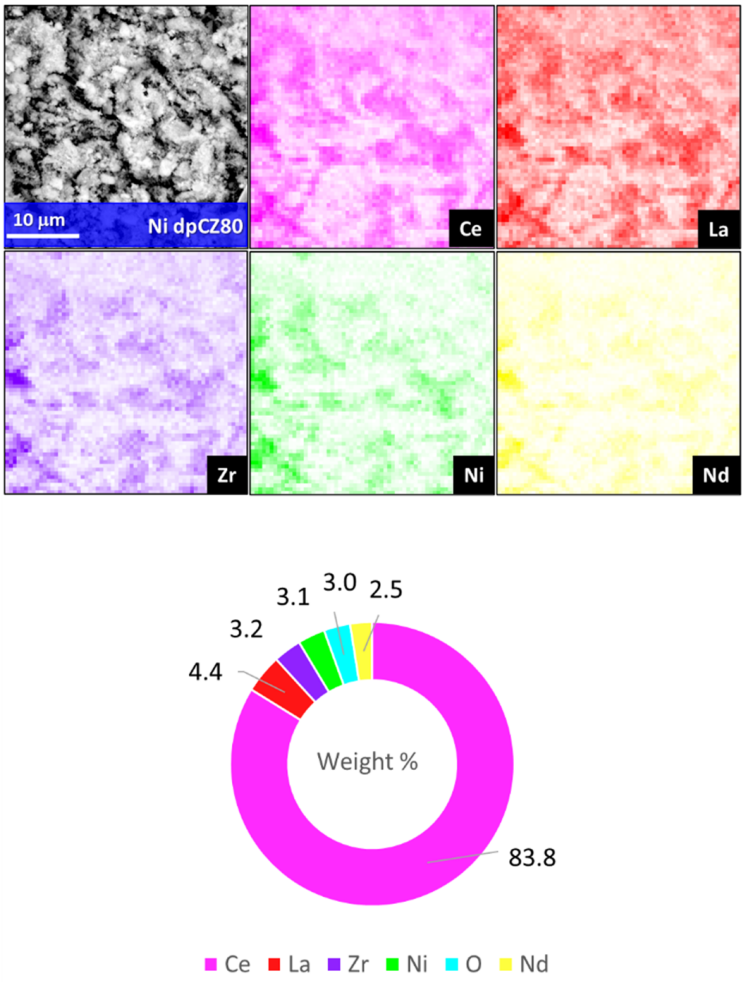

Figure 4. EDX mapping of elements distribution over the NidpCZ80 catalyst.

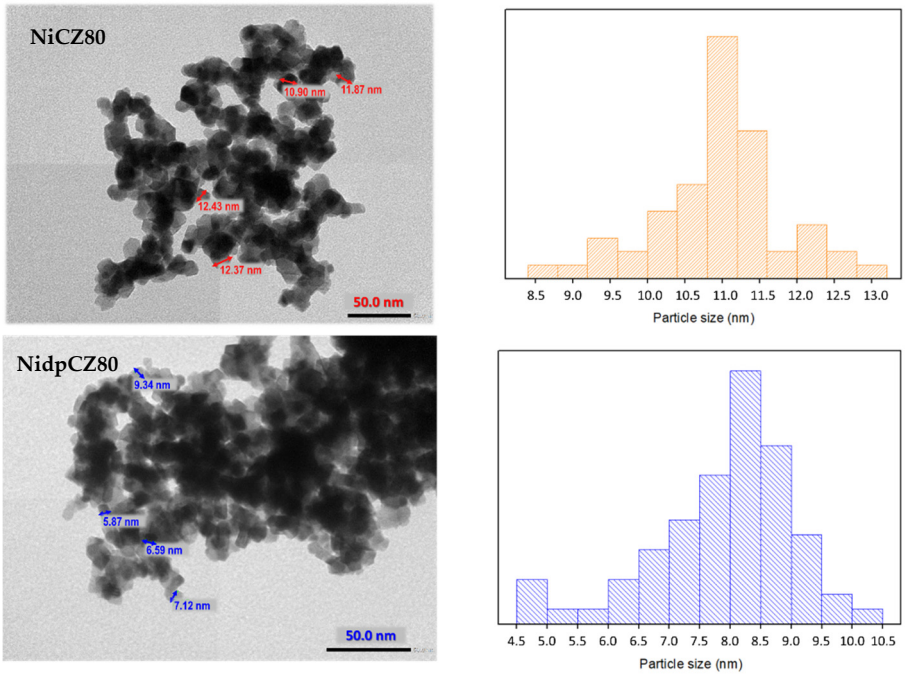

Figure 5. TEM images and particle size distribution of catalysts.

The TPR-H_2 profiles of supports, undoped and doped, and Ni-catalysts are shown in Figure 6. The TPR-H_2 curve of bare supports features two peaks since the reduction occurs in two steps. In detail, the lower temperature is related to the reduction of superficial Ce^{4+} and Zr^{x+}, while the larger band up to 700 °C is the result of the progressive release of the lattice oxygen from the bulk of the sample. The doped support is characterized by a similar profile, in agreement with Sartoretti et al. [17]. The same behavior is also observed for both Ni supported catalysts, NiCZ80 and NidpCZ80. In particular, for the catalyst supported on the doped support, peaks ascribed to the direct reduction of NiO to Ni are shifted to lower temperatures.

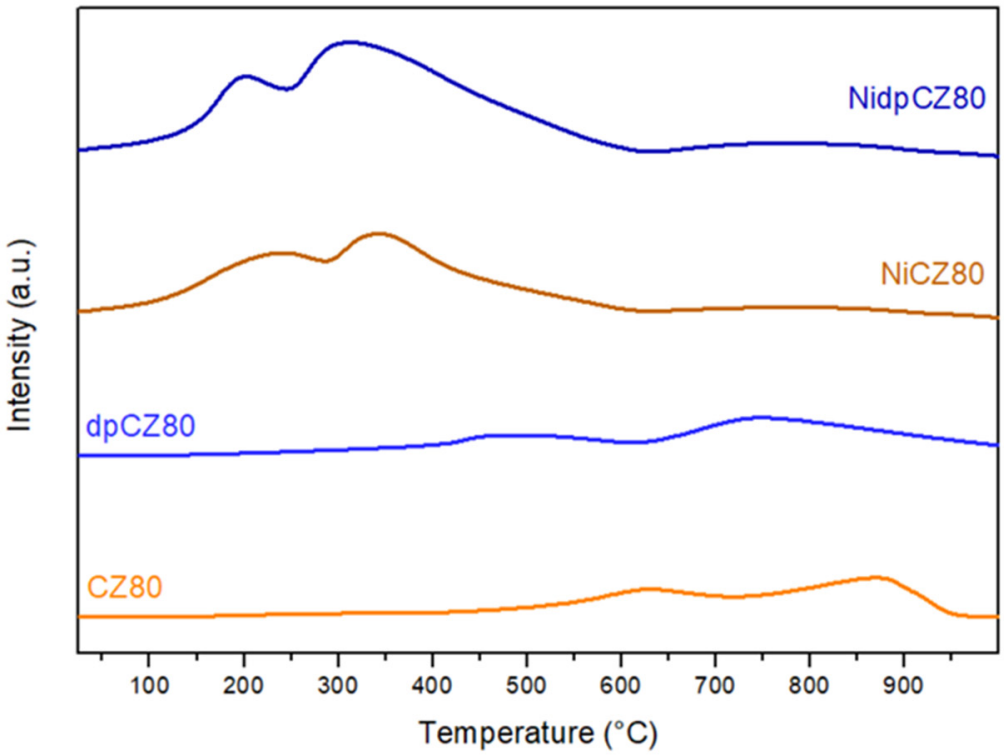

Figure 6. H_2-TPR profiles of supports (undoped CZ80 and doped dpCZ80) and Ni supported catalysts, NiCZ80 and NidpCZ80.TPR.

2.2. Catalytic Test Results

2.2.1. Methane as Fuel

The autothermal reforming (ATR) of methane at 800 °C involves a thermal energy balance between the endothermic reaction of steam reforming (SR—Equation (1)) and the exothermic reaction of partial oxidation (POX—Equation (2)):

$$CH_4 + H_2O \rightleftharpoons CO + 3H_2,\ \Delta H^\circ \simeq 226\ kJ;\ \Delta G^\circ \simeq -45\ kJ\ at\ 800\ ^\circ C \quad (1)$$

$$CH_4 + \frac{1}{2}O_2 \rightleftharpoons CO + 2H_2,\ \Delta H^\circ \simeq -22\ kJ;\ \Delta G^\circ \simeq -234\ kJ\ at\ 800\ ^\circ C \quad (2)$$

Therefore, the overall reaction equation for the autothermal process is:

$$CH_4 + xH_2O + 2(1-x)H_2O \rightleftharpoons CO_2 + 2(2-X)H_2,\ \Delta H^\circ \simeq 0\ J;\ \Delta G^\circ \simeq -192\ kJ\ at\ 800\ ^\circ C \quad (3)$$

The performance in terms of CH_4 conversion (average values), in different reaction conditions, is shown for both undoped and doped catalysts in Figure 7.

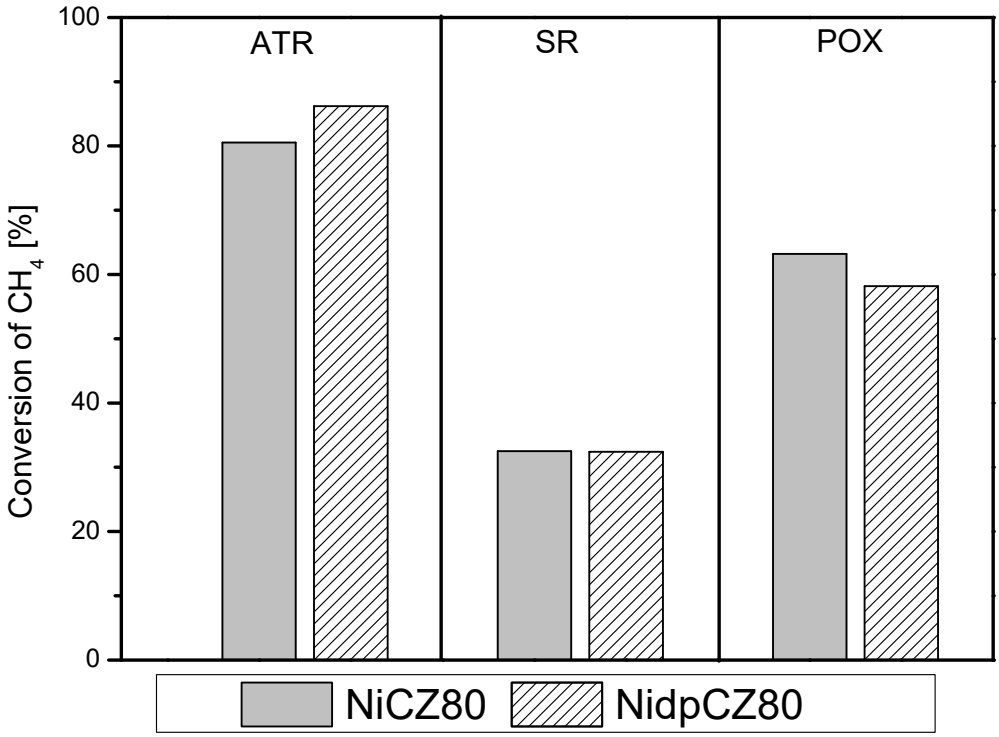

Figure 7. Conversion of methane CH_4 for NiCZ80 and NidpCZ80 under ATR, SR, and POX conditions at T = 800 °C GSVH = 120,000 h^{-1}.

The better performance in terms of conversion was related to the reaction under the ATR condition, for both catalysts. This could probably be due to the acknowledged indirect mechanism of ATR, according to which oxidation of CH_4 occurs producing carbon dioxide and water and, then, the unreacted CH_4 produces synthesis gas via carbon dioxide and steam-reforming reaction [19]. Moreover, in our previous works we have observed the better performance of ATR and POX conditions with respect to SR condition, in which the catalytic performance is highly depleted by hydration. At high temperatures, as well as 800 °C, a high-water saturation grade of reaction systems occurs, reducing active site accessibility with negative consequences on the catalytic performances [20].

The ATR conversion of methane on doped catalyst is slightly improved by the presence of the doping elements; on the other hand, no significant differences promoted by doping are observed for the SR of methane. Instead, in the POX condition, the doping seems to have a detrimental effect.

Since the conversion of fuels is quite stable in the time on stream considered, as shown in Figure 8, it is possible to calculate the average value of the products formed during the different reactions. By Figure 8, it is possible to notice that the product distribution depends on the reaction conditions. The largest amount of H_2 is obtained in the ATR reaction conditions; on the other hand, the largest amount of CO is obtained in the POX reaction conditions. The conversion value obtained for the ATR of methane is comparable or higher than values reported in literature, even for catalysts at higher nickel contents, as shown in Table 1.

The spent catalysts were characterized by XRD to identify possible structural modifications and/or formation of surface carbon species. No evident alterations of the support structure were observed, and all patterns were similar to those reported, as an example, in Figure S1.

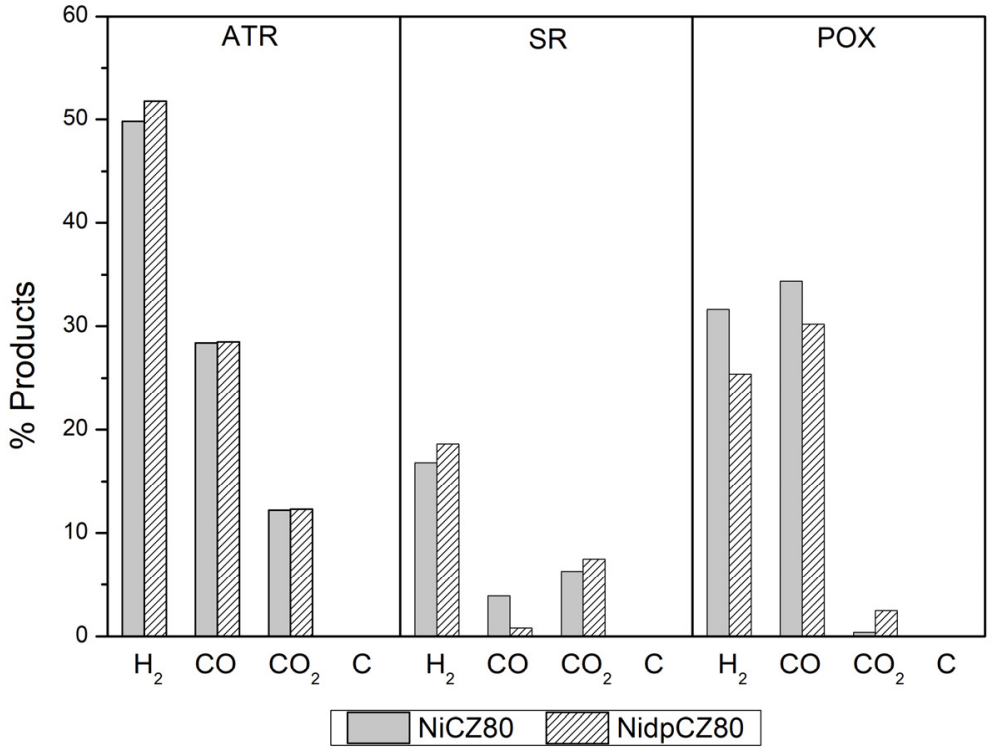

Figure 8. Products distribution for NiCZ80 and NidpCZ80 under ATR, SR, and POX conditions of methane at T = 800 °C, GSVH = 120,000 h^{-1}.

Table 1. List of the average conversion values of different fuels examined in ATR conditions on doped and undoped catalysts.

Catalyst	Ni Content wt/wt%	Composition of Inlet Feed	Duration of Test	Space Velocity	Methane Conversion %	H_2 Yield	Ref.
$Ni/CeZrO_2$	10%	$2CH_4/1H_2O/0.5O_2$	25 h	12 $mg_{catalyst}$/ 180 mL/min	50 at 800 °C	40%	[21]
$Ni/Ce_{0.5}Zr_{0.5}O_2$	10%	$2CH_4/1H_2O/0.5O_2$	24 h	12 $mg_{catalyst}$/ 180 mL/min	50 at 800 °C	90%	[22]
$NiPd/20La_2O_3/10Ce_{0.5}Zr_{0.5}O_2/Al_2O_3$	10%(Ni) 0.5%(Pd)	$1CH_4/1H_2O/0.75O_2$	27 h	–	97 at 850 °C	69%	[23]
$Ni/Cu_{0.05}Ce_{0.2}Zr_{0.1}Al_{0.65}O_x$	10%	$1CH_4/0.5O_2/2.5H_2O$	–	4800 h^{-1}	83 at 650 °C	–	[24]
Ni-modified LSFCO/CGO	10%	$C_3H_8/0.5O_2/2.5H_2O$	100 h	120,000 h^{-1}	95 at 800 °C	50% (mean value)	[20]
Ni/MgAl	15%	$C_3H_8/0.37O_2/3H_2O$	–	9600 mL/g_{cat} h	100 at 700 °C	55%	[25]
NidpCZ80	3%	$1CH_4/0.5O_2/2.5\ H_2O$	10 h	120,000 h^{-1}	86.4 at 800 °C	52%	This work
NiCZ80	3%	$1CH_4/0.5O_2/2.5\ H_2O$	10 h	120,000 h^{-1}	80 at 800 °C	48%	This work

2.2.2. Propane as Fuel

Propane auto thermal reforming proceeds combine the POX conditions (Equation (4)) and SR condition (Equation (5)):

$$C_3H_8 + 3/2O_2 = 3CO + 4H_2\ \Delta H = -227.6\ kJ\ mol^{-1} \quad (4)$$

$$C_3H_8 + 3H_2O = 3CO + 7H_2\ \Delta H = 498\ kJ\ mol^{-1} \quad (5)$$

However, other reactions can occur as hydrogenation/decomposition of unsaturated C_3H_x species [24].

Figure 9 shows the Ni supported catalysts' performance in the propane reaction conversion. Under ATR condition the propane conversion is very high for the two

catalysts, suggesting that the combination of the steam and oxygen in the reagent stream plays a decisive role in promoting catalyst activity and stability. In the SR and POX conditions, the doped catalyst exhibits higher conversion with respect to the undoped one. For both catalysts, products distribution is affected by operating conditions. In accordance with our previous works, in the POX condition, the production of H_2 is lower than ATR and SR conditions [20].

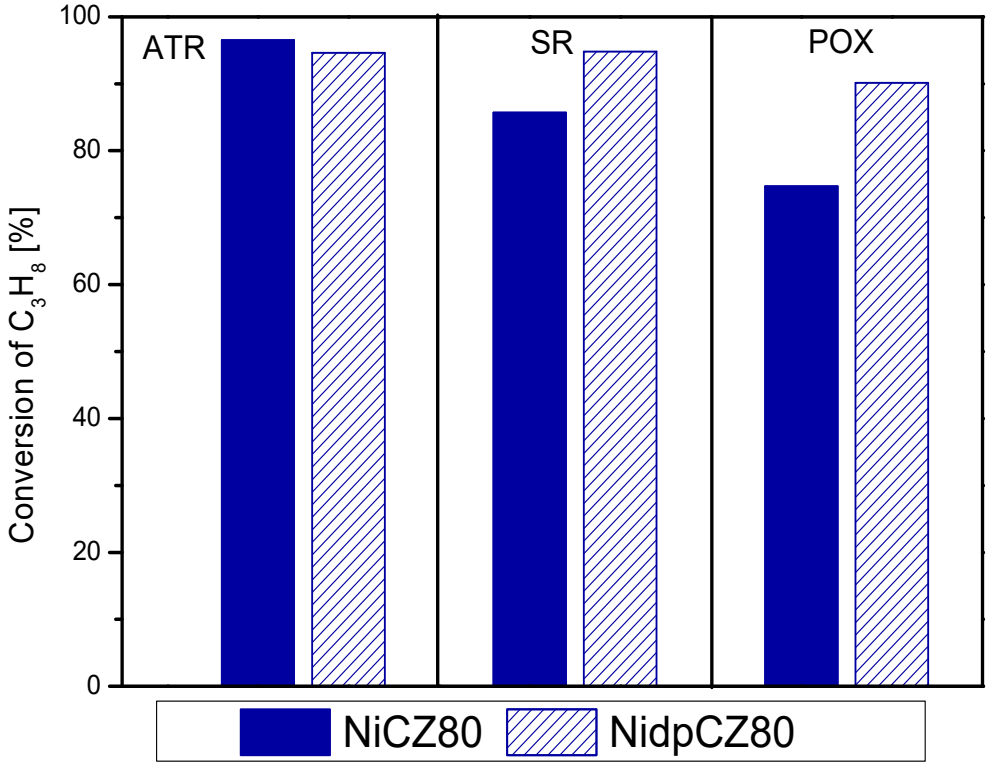

Figure 9. Conversion of methane CH_4 for NiCZ80 and NidpCZ80 under ATR, SR, and POX conditions at T = 800 °C GSVH = 120,000 h^{-1}.

Moreover, there is an enhanced production of CH_4 and C_2H_4 due to a significant decomposition of propane [26] and other products (C+ others), probably due to oxygenated molecules that cannot be revealed by the analytical equipment used.

The distribution of products is presented in Figure 10. Under the ATR condition, the distribution of products is not substantially modified by the doping of the support. Both catalysts, undoped and doped, show the highest H_2 content in the SR condition. In addition, in the SR condition, the effect of doping is remarkable in the lower methane production and in the higher C_2H_6 content for the reaction catalyzed by the Ni catalyst with doped support. The formation of methane probably does not occur by hydrogenation/ decomposition of unsaturated species and methane can be formed by methanation of carbon oxides and/or hydrogenolysis of propane.

2.2.3. Odorized Fuel with H_2S

The sulfur tolerance is one of the fundamental properties that a reforming catalyst must possess to ensure high reaction process efficiency, especially if biofuels are used.

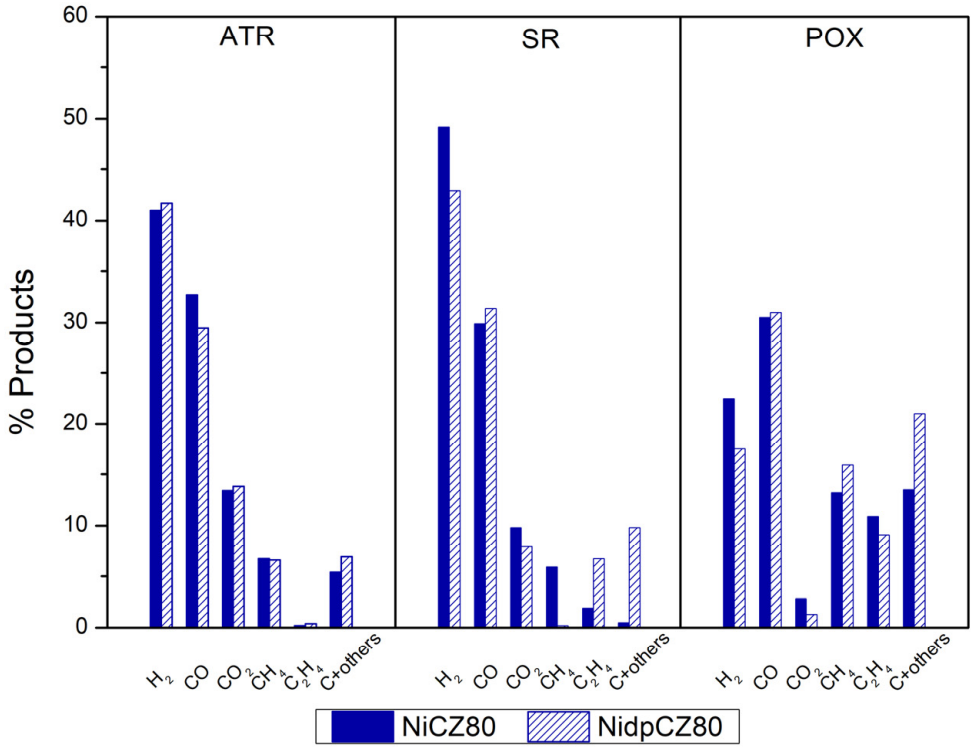

Figure 10. Product distribution for NiCZ80 and NidpCZ80 under ATR, SR and POX conditions of methane at T = 800 °C, GSVH = 120,000 h^{-1}.

Biogas contains CH_4 and CO_2 as its main components and among of other gases, hydrogen sulfide (e.g., H_2S, NH_3, and H_2) is a problematic contaminant because it can poison the reforming catalyst. The H_2S concentration is affected by the type of feedstocks/waste sources utilized to produce biofuels. Only 10 ppm of H_2S can deactivate the nickel catalyst, but temperature, reaction time, and catalyst geometry have a significant impact on the stability of the catalyst [27]. The irreversible chemisorption of sulfur onto catalytic active sites is the primary cause of catalyst deactivation. Due to its high adsorption strength relative to other species competing for catalytic sites in the reaction media, sulfur has a poisonous effect. The direct use of odorized propane, particularly in non-conventional energy conversion technologies, such as solid oxide fuel cells, causes particular problems [28]. Actually, conventional SOFCs cannot prevent coke formation from organic fuels nor are they resistant to sulfur poisoning [27]. These restrictions can be circumvented by utilizing fuel processing consisting of a purification process in the first step and reforming of fuel to syngas in the second step, with an obvious increase in the system's complexity and cost [29]; furthermore, the risk of poisoning cannot be eliminated entirely [30]. Using novel catalytic materials, able to prevent the formation of coke and, simultaneously, to resist to sulfur poisoning, is one possible response to such requirements. The promotion of supports with proper elements can increase the catalyst's basicity and its poison resistance related to sulfur components. With this background, catalytic tests of autothermal reforming were carried out over undoped and doped catalysts, in the presence of 100 ppm of H_2S. A different catalytic activity is observed for the different fuels as shown in Figure 11. In particular, in the presence of H_2S, a dramatic collapse in the conversion was detected using methane and biogas as fuels, for both catalytic systems. This can be due to the Ni sulfide species formation, on the catalyst surface, that results in a decrease in available catalytic sites. In the case of propane, the loss of conversion is moderate for both catalysts.

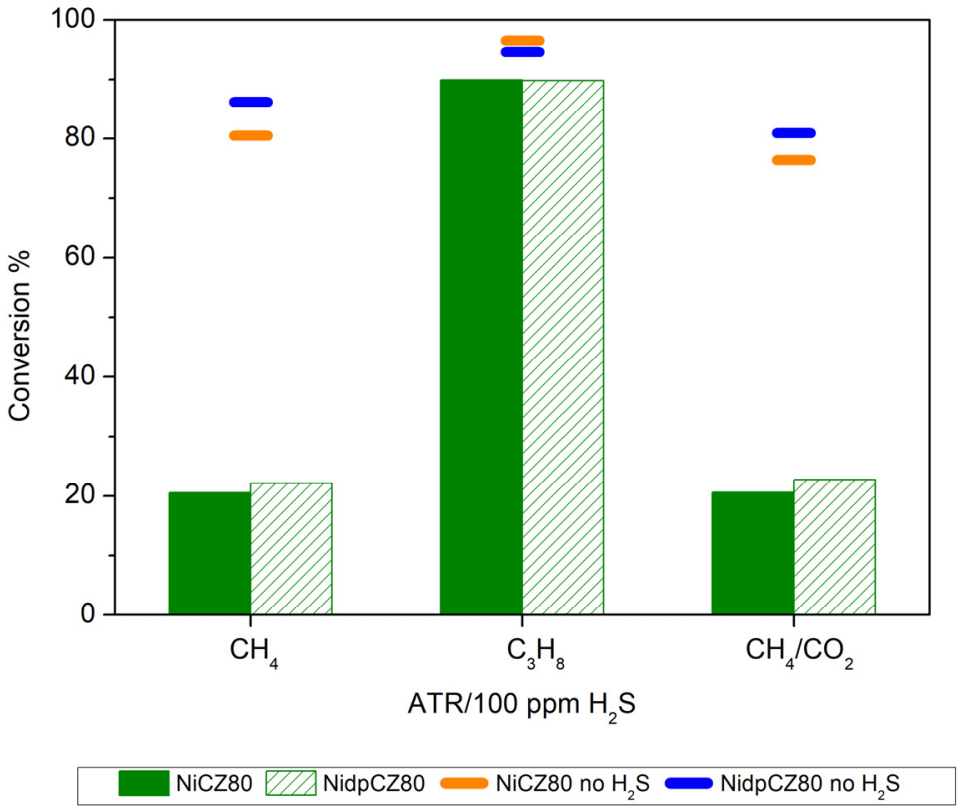

Figure 11. Conversion of different fuels in ATR conditions at T = 800 °C GSVH = 12,000 h^{-1} over undoped and doped catalysts.

The different behavior in the loss of conversion for different fuels is explained considering that the addition of H_2S, that, as stated above, tended to block the catalytic sites, makes the oxidation reaction of fuels less favored than in the case of the ATR carried out in the absence of H_2S. Instead, the catalytic cracking process became the most favored reaction. This find is also confirmed by the highest yield of H_2 and CO, obtained in the absence of H_2S (around three times higher). The addition of H_2S in the ATR of propane causes more production of CO_2, CH_4 and C_2H_4 for both doped and undoped catalytic systems (Figure S2). Despite how the sulfur presence affected the product distribution, however, no severe catalysts deactivation occurred.

The spent catalysts were characterized by XRD in order to identify possible structural modifications and/or formation of surface carbon species. No evident modifications of the support structure were observed, all patterns were similar to those reported for fresh catalysts (Figure S3), probably due to a limit of detection of the instrument used. Then, to investigate more in-depth the presence and the amount of coke, thermogravimetric analysis (TGA-DSC) was employed to estimate the amount of deposited carbon. The content of carbon for all catalytic systems was lower than 3%. The higher amount of coke (2.8 wt%) was detected for the undoped catalyst after ATR of odorized propane with respect to the doped catalysts (0.39 wt%). The amount of carbon detected on the catalysts used for the other reactions was lower than 0.2%.

TEM images (Figure S4) confirm the absence of coke for the catalytic system tested under the ATR of methane on the doped catalyst and highlighted the high sintering of the catalyst that probably produced the loss of conversion in undoped and doped catalysts. The random presence of carbon nanotubes (Figure S5) was detected in the ATR of propane with undoped catalysts, confirming the low content of carbon detected by thermogravimetric analysis and the preserved activity in the considered time of reaction.

Based on this observation, the catalytic system obtained over the doped catalyst resulted in high resistance to deactivation, being characterized by a higher concentration of defect groups and oxygen vacancies (due to the doping of neodymium and lanthanum), thereby preventing the formation of deactivating species (amorphous carbon and nickel sulfide).

2.2.4. Endurance Test

Endurance tests of undoped NiCZ80 and doped NidpCz80 catalysts were carried out under ATR of C_3H_8 conditions in the presence of 100 ppm of H_2S. The profiles of conversion are reported in Figure 12. As shown, the undoped catalyst exhibited catalytic activity for around 55 h. After that, a dramatic loss of conversion was registered, probably due to the coke formation that hindered the gas flow, causing the block of the reaction. In effect, as shown in Figure S6, the reactor was full of coke. Instead, the doped catalyst showed stable catalytic activity for over 100 h.

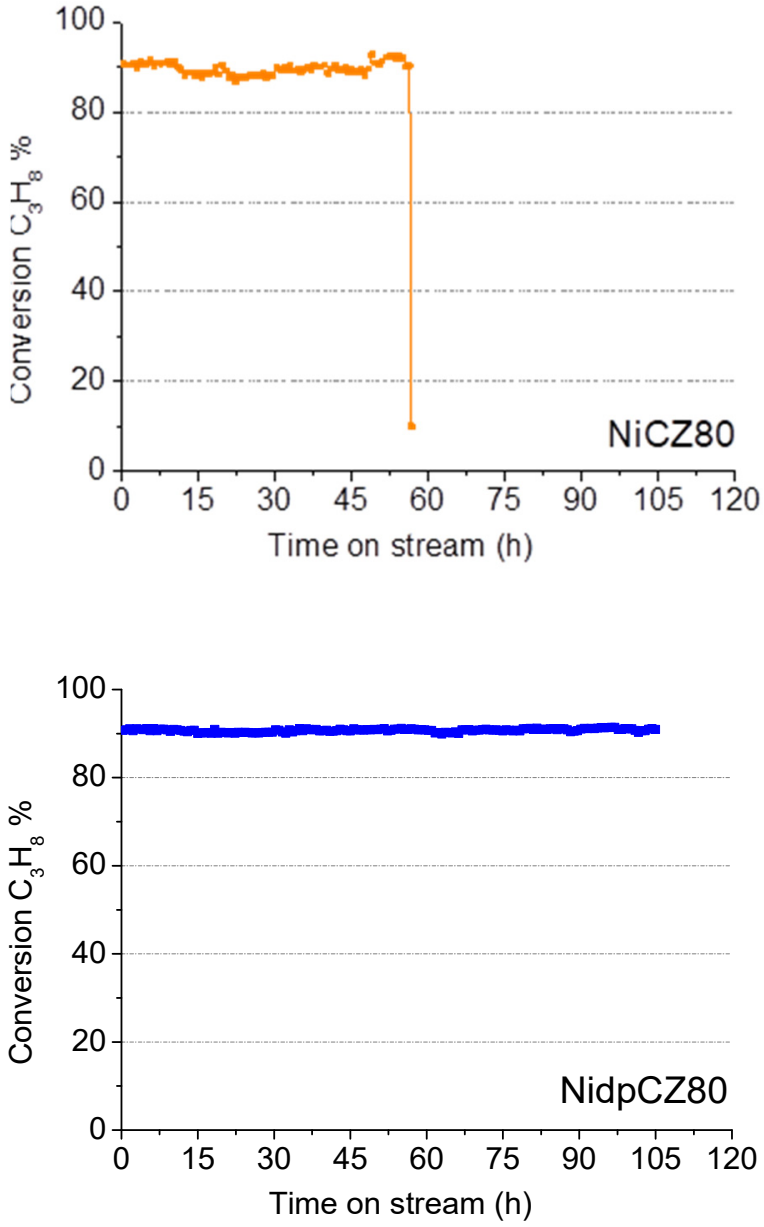

Figure 12. Profiles of C_3H_8 conversion for NiCZ80 and NidpCZ80 under ATR conditions at T = 800 °C and GSHV = 120,000 h^{-1}.

The characterization of spent catalysts was carried out by XRD and TG-DSC analysis in order to identify the coke formed during reactions. XRD results of spent catalysts doped and undoped are shown in Figures 13 and 14, respectively. For both catalysts, peaks attributable to the carbon formation in the 2θ range 25–27° were clearly observed, even if they were characterized by different profiles. In the case of the undoped NiCZ80 catalyst, the peak was sharper than that of the doped NidpCZ80 and the corresponding d_{002} value (3.432 Å) approaches the theoretical value of standard graphite (3.354 Å) [31].

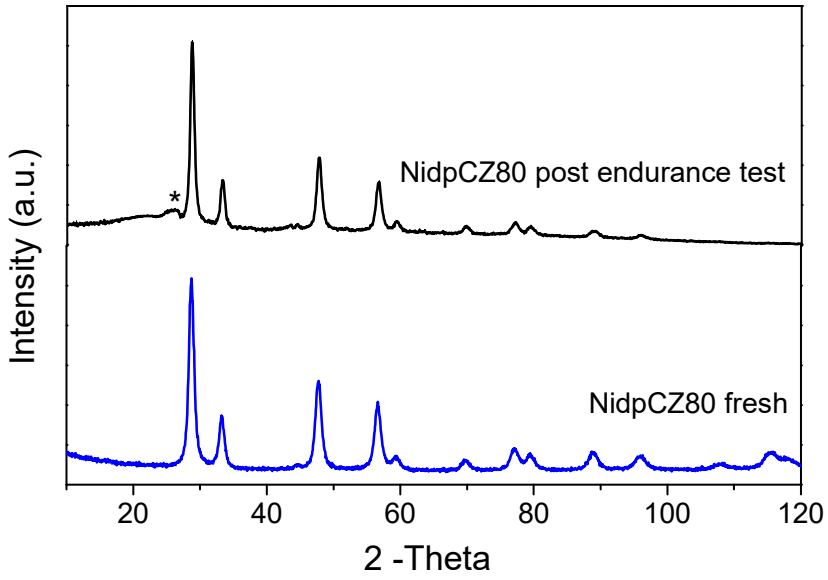

Figure 13. X-ray diffraction spectra of NidpCZ80 catalyst, fresh and after endurance test.

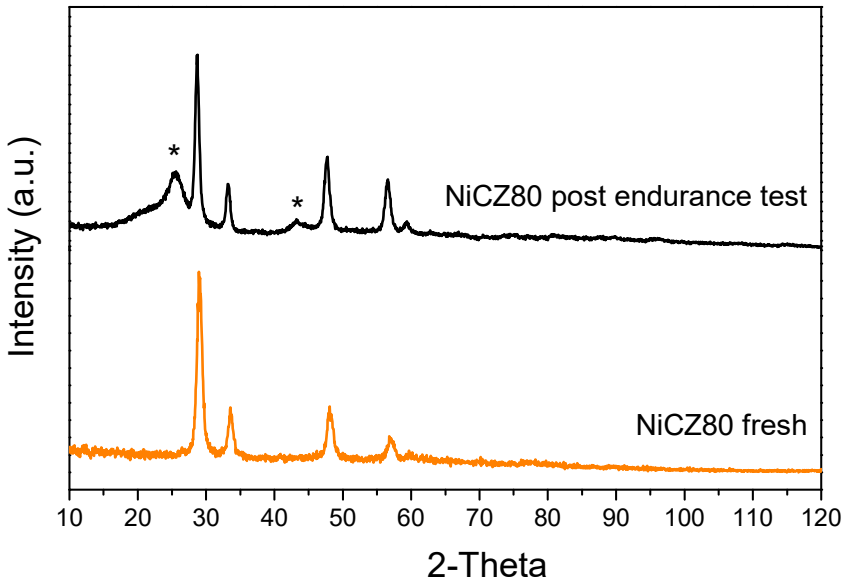

Figure 14. X-ray diffraction spectra of NiCZ80 catalyst, fresh and after endurance test.

The value of d_{002} (3.395 Å) for the peak of the doped catalyst was far from the theoretical value, so amorphous carbon instead of ordered graphite was obtained. As is well known, the nature of coke formed during the reaction influences the deactivation of catalysts [32]. Therefore, some forms of carbon reduce the catalytic activity and others do not. For high temperatures (>650 °C) graphitic carbon species were formed over the undoped catalyst, encapsulating the metallic surface [32]. The above observation on coke formation led to the conclusion that doping addresses the methanation to be a coke-insensitive reaction. The

catalytic activity of the doped catalyst was not affected even when appreciable quantities of "coke" were deposited on its surface, as proved by thermogravimetry curve, Figure 15. It was probably due to the promotion effect of La and Nd being able to maintain the surface reactive enough [33].

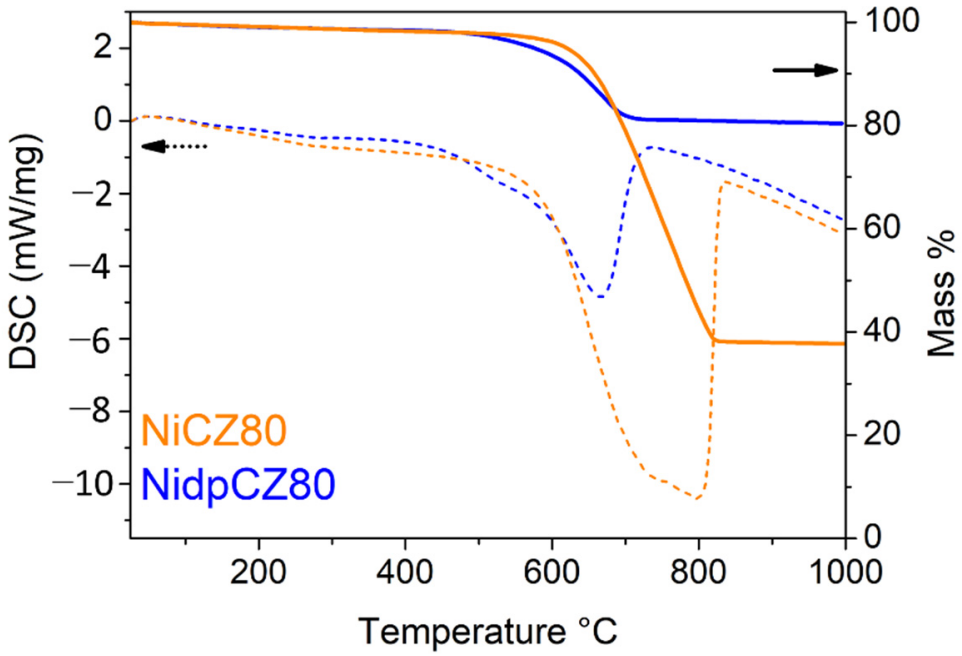

Figure 15. TGA-DSC profiles of NidpCZ80 and NiCZ80 catalysts after endurance test.

3. Materials and Methods

3.1. Catalytic System

$Ce_{0.8}Zr_{0.2}O_2$ and $Ce_{0.8}Zr_{0.13}La_{0.05}Nd_{0.02}O_{2-x}$ were prepared as reported in our previous work [18]. Briefly, proper amounts of $RE(NO_3)_3{\cdot}6H_2O$ salt (RE = Ce^{3+}, La^{3+}, Nd^{3+}; Treibacher Industrie AG) and $ZrO(NO_3)_2$ liquid gel (Treibacher Industrie AG) were dissolved in demineralized water, obtaining a 0.2 M solution; concentrated H_2O_2 (35% Sigma-Aldrich—Italy) was then added according to the molar ratio $[H_2O_2]$/[tot metals ions] equal to 3. After 45 min of stirring at room temperature, concentrated $NH_3 \bullet H_2O$ (28% Sigma-Aldrich—Italy) was added to obtain a pH value of 10.5. Finally, lauric acid (Sigma-Aldrich—Italy), using a molar ratio ([tot metal ions]/[lauric acid]), equal to 0.25, was added in solid form in the batch and maintained under continuous stirring for 4 h. The precipitate was then filtered and washed three times with 0.5 L of demineralized water and the resulting cake was dried at 100 °C overnight. The dry precipitate was calcined in air at 500 °C for 4 h. The obtained supports were impregnated with a solution of nickel nitrate hexahydrate solubilized in ethanol and successively calcined under air flux at 500 °C for 1 h. The nominal content of nickel is 3.5% in weight with respect to the support.

In order to evaluate the thermal stability of the catalyst, XRD spectra versus increasing temperatures in the range 25–1000 °C were collected by a Panalytical Empyrean S-2 diffractometer, using Cu Kα radiation (1.54056 Å) at 40 kV and 40 mA. The patterns were recorded in step scan mode from 10–60° 2θ angles in steps of 0.02° and a count time of 5 s per step.

The SEM-EDX analysis was carried out to acquire information about the morphological and compositional configurations. To this purpose, a Phenom Pro-X scanning electron microscope equipped with an energy-dispersive X-ray spectrometer was utilized. The EDX analysis was used to evaluate the content and dispersion of metal, acquiring for all samples at least 20 points of investigation at three different magnifications. The counting time for the EDX analysis was 120 s. The results were found to be reproducible to less than ±5% for all samples.

Temperature-programmed reduction (TPR) experiments were carried out in an AutoChem II 2920 analyzer (Micromeritics) using a 5% H_2 in nitrogen mixture flowing at 35 mL/min (STP). For TPR measurements, the temperature was increased from 50 to 950 °C at a heating rate of 10 °C min^{-1}. Each sample (50 mg) was treated at 500 °C for 1 h in an air flow (50 mL min^{-1}) before the analysis.

The deposited carbon content was evaluated by means of thermogravimetric (TGA-DSC) (Netzsch). The temperature-programmed experiments were carried out in the range 25–1000 °C, under a total air flow rate of 100 cc/min with a heating rate of 2 °C min^{-1}.

Finally, transmission electron microscopy (TEM) analysis was performed using a JEOL 1400 Plus instrument operated at 120 kV, able to achieve a 0.19 nm point-to-point resolution and a 0.14 nm line resolution.

3.2. Catalytic Activity Measurements

The catalytic activity was evaluated in a quartz microreactor (internal diameter = 4 mm) positioned in a ceramic tube furnace, at atmospheric pressure and at the temperature of 800 °C.

All catalytic tests were performed at 120,000 h^{-1} space velocity (GHSV). The gaseous mixture flows were adjusted for the different reactions: SR (steam to carbon mole fraction S/C = 2.5); POX (oxygen to carbon mole fraction O/C = 0.5); ATR (mole fraction S/C = 2.5 and O/C = 0.5). Some experiments were carried out with 100 ppm of H_2S. In order to take into account the variation of the number of moles in the reactions, nitrogen was fed into the inlet stream and then was used as an internal standard. The outlet stream of the reactor was analyzed by gas-chromatography equipped with a TCD detector and columns appropriate for the gas identification. The time on stream was ten hours and the catalytic activity results were generally registered 15 min after the start of reaction. Overall carbon and hydrogen balances were close to 100% in each experiment with standard deviation lower than 3%. Catalytic tests performed are summarized in Table S1 (reported in the supplementary information) together with the related operational conditions.

Conversion percentages were calculated by means of the following equation:

$$\%Conversion = \frac{Fuel_{in} - Fuel_{out}}{Fuel_{in}}$$

4. Conclusions

The reactivity of the nickel catalytic systems with defined ceria zirconia compositions, undoped and doped with lanthanum and neodymium $Ce_{0.8}Zr_{0.2}O_2$ (CZ80) and $Ce_{0.8}Zr_{0.13}La_{0.5}Nd_{0.2}O_{2-x}$ (dpCZ80), were tested towards the reforming reactions: steam reforming, partial oxidation and autothermal reforming of different fuels, such as methane, biogas, and propane. Catalysts were extensively characterized by various analytical techniques, highlighting (i) the insertion of lanthanum and neodymium into the fluorite structure, (ii) the homogeneity distribution of the different elements in the catalysts, and (iii) the loading of the metallic phase very close to the nominal content (3.5 ± 0.2%). Undoped and doped catalysts showed both a well-defined cubic nanomorphology with slightly reduced dimension for the doped sample, together with the absence of the segregation related to lanthanum and neodymium doping. The effect of doping on the reducibility of the catalyst seemed to be limited to the slight anticipation of the surface reduction at low temperatures. As shown, the doped catalyst just slightly improved the ATR conversion of methane, while no significant differences were promoted by doping elements for the SR of methane and in the POX conditions, where the doping seemed to have a detrimental effect. With regard to propane conversion, under ATR condition, it was very high for both catalysts, suggesting that the combination of steam and oxygen in the reagent stream plays a decisive role in promoting catalyst activity and stability. In the SR and POX conditions, higher conversions were registered for the doped catalyst compared to undoped one. The doped catalyst dispersed nickel species on the surface with a higher concentration of defect groups and oxygen vacancies (due to neodymium and lanthanum doping), thereby preventing the formation of deactivating species (amorphous carbon and nickel sulfide) and resulting in a

higher resistance to deactivation. An endurance catalytic test confirmed the beneficial effect of the doped catalysts. Further developments will be interested in the scale up of powdered catalyst on structured form that will be tested as anode catalysts for SOFCs/SOECs systems.

Supplementary Materials: The following supporting information can be downloaded at: https://www.mdpi.com/article/10.3390/catal13010165/s1. Table S1: Experimental conditions adopted for ATR, SR and ATR reactions over undoped NiCZ80 and doped NidpCZ80 catalysts. Figure S1: XRD spectra of NiCZ80 spent catalyst after methane SR, POX and ATR reactions. Figure S2: Conversion of propane in ATR, SR and POX conditions at T = 800 °C GSVH = 12,000 h^{-1} over undoped and doped catalysts, with and without 100 ppm H_2S. Figure S3: X-ray patterns of NidCZ80 fresh and after ATR reactions of methane and propane with 100 ppm of H_2S at T = 800 °C and GSVH = 120,000 h^{-1}. Figure S4:TEM image of doped catalysts after ATR of methane at T = 800 °C and GSHV = 120,000 h^{-1}. Figure S5: TEM image of undoped catalysts after ATR of propane at T = 800 °C and GSHV = 120,000 h^{-1}. Figure S6: Reactors after endurance tests of undoped NiCZ80 and doped NidpCz80. The presence of coke is evident for the undoped NiCZ80 catalyst.

Author Contributions: P.F., A.M. (Angela Malara), M.B., M.M. and A.P. (conceptualization, methodology, investigation, formal analysis); P.F., A.M. (Angela Malara), L.B. and A.M. (Anastasia Macario) (writing—original draft preparation, writing—review and editing, data curation, supervision, project administration, funding acquisition); A.T. and P.L.A. (supervision, funding acquisition). All authors have read and agreed to the published version of the manuscript.

Funding: This research was funded by the project PRIN 2017 "DIRECTBIOPOWER", for the development of innovative components for IT-SOFC (Funding: MIUR; Funding Number 201FCFYHK_002).

Conflicts of Interest: The authors declare no conflict of interest.

References

1. IPCC. *Mitigation of Climate Change*; Working Group III contribution to the Fifth Assessment Report; IPCC: Geneva, Switzerland, 2014; Volume 1454, p. 147.
2. Asghar, M.I.; Jouttijärvi, S.; Jokiranta, R.; Lund, P.D. Remarkable ionic conductivity and catalytic activity in ceramic nanocomposite fuel cells. *Int. J. Hydrogen Energy* **2018**, *43*, 12892–12899. [CrossRef]
3. Brett, D.J.L.; Atkinson, A.; Brandon, N.P.; Skinner, S.J. Intermediate temperature solid oxide fuel cells. *Chem. Soc. Rev.* **2008**, *37*, 1568–1578. [CrossRef] [PubMed]
4. Kilner, J.A.; Burriel, M. Materials for intermediate-temperature solid-oxide fuel cells. *Annu. Rev. Mater. Res.* **2014**, *44*, 365–393. [CrossRef]
5. Park, S.; Vohs, J.M.; Gorte, R.J. Direct oxidation of hydrocarbons in a solid-oxide fuel cell. *Nature* **2000**, *404*, 265–267. [CrossRef] [PubMed]
6. Irshad, M.; Siraj, K.; Raza, R.; Ali, A.; Tiwari, P.; Zhu, B.; Rafique, A.; Ali, A.; Kaleem Ullah, M.; Usman, A. A brief description of high temperature solid oxide fuel cell's operation, materials, design, fabrication technologies and performance. *Appl. Sci.* **2016**, *6*, 75. [CrossRef]
7. Frontera, P.; Modafferi, V.; Frusteri, F.; Bonura, G.; Bottari, M.; Siracusano, S.; Antonucci, P.L. Catalytic features of Ni/Ba–Ce0. 9–Y0. 1 catalyst to produce hydrogen for PCFCs by methane reforming. *Int. J. Hydrog. Energy* **2010**, *35*, 11661–11668. [CrossRef]
8. Ettler, M.; Timmermann, H.; Malzbender, J.; Weber, A.; Menzler, N.H. Durability of Ni anodes during reoxidation cycles. *J. Power Sources* **2010**, *195*, 5452–5467. [CrossRef]
9. Ru, Y.; Sang, J.; Xia, C.; Wei, W.-C.J.; Guan, W. Durability of direct internal reforming of methanol as fuel for solid oxide fuel cell with double-sided cathodes. *Int. J. Hydrog. Energy* **2020**, *45*, 7069–7076. [CrossRef]
10. Xi, X.; Abe, H.; Naito, M. Effect of composition on microstructure and polarization resistance of solid oxide fuel cell anode Ni-YSZ composites made by co-precipitation. *Ceram. Int.* **2014**, *40*, 16549–16555. [CrossRef]
11. Mehran, M.T.; Khan, M.Z.; Lee, S.-B.; Lim, T.-H.; Park, S.; Song, R.-H. Improving sulfur tolerance of Ni-YSZ anodes of solid oxide fuel cells by optimization of microstructure and operating conditions. *Int. J. Hydrog. Energy* **2018**, *43*, 11202–11213. [CrossRef]
12. Costa-Nunes, O.; Gorte, R.J.; Vohs, J.M. Comparison of the performance of Cu–CeO_2–YSZ and Ni–YSZ composite SOFC anodes with H_2, CO, and syngas. *J. Power Sources* **2005**, *141*, 241–249. [CrossRef]
13. Escudero, M.J.; Valero, C.; Cauqui, M.Á.; Goma, D.; Yeste, M.P. Ni-Ce-ZrO_2 system as anode material for direct internal reforming biogas solid oxide fuel cells. *Fuel* **2022**, *322*, 124247. [CrossRef]
14. Osazuwa, O.U.; Abidin, S.Z. An overview on the role of lanthanide series (rare earth metals) in H2 and syngas production from CH4 reforming processes. *Chem. Eng. Sci.* **2020**, *227*, 115863. [CrossRef]
15. Liu, H.; Li, Y.; Wu, H.; Yang, W.; He, D. Effects of Nd, Ce, and La modification on catalytic performance of Ni/SBA-15 catalyst in CO_2 reforming of CH_4. *Chin. J. Catal.* **2014**, *35*, 1520–1528. [CrossRef]

16. Dedov, A.G.; Loktev, A.S.; Komissarenko, D.A.; Mazo, G.N.; Shlyakhtin, O.A.; Parkhomenko, K.V.; Kiennemann, A.A.; Roger, A.-C.; Ishmurzin, A.V.; Moiseev, I.I. Partial oxidation of methane to produce syngas over a neodymium–calcium cobaltate-based catalyst. *Appl. Catal. A Gen.* **2015**, *489*, 140–146. [CrossRef]
17. Sartoretti, E.; Novara, C.; Chiodoni, A.; Giorgis, F.; Piumetti, M.; Bensaid, S.; Russo, N.; Fino, D. Nanostructured ceria-based catalysts doped with La and Nd: How acid-base sites and redox properties determine the oxidation mechanisms. *Catal. Today* **2022**, *390*, 117–134. [CrossRef]
18. Pappacena, A.; Graziutti, R.; Boaro, M.; Trovarelli, A. CeO_2-ZrO_2 catalysts for the use of biogas in IT-SOFC. *ECS Trans.* **2015**, *68*, 2789–2795. [CrossRef]
19. Nguyen, T.G.H.; Sakamoto, M.; Uchida, T.; Doan, D.C.T.; Dang, M.C.; Tu, P.H.; Sasaki, K.; Shiratori, Y. Development of paper-structured catalyst for application to direct internal reforming solid oxide fuel cell fueled by biogas. *Int. J. Hydrog. Energy* **2019**, *44*, 10484–10497. [CrossRef]
20. Lo Faro, M.; Modafferi, V.; Frontera, P.; Antonucci, P.; Aricò, A.S. Catalytic behavior of Ni-modified perovskite and doped ceria composite catalyst for the conversion of odorized propane to syngas. *Fuel Process. Technol.* **2013**, *113*, 28–33. [CrossRef]
21. Dantas, S.C.; Escritori, J.C.; Soares, R.R.; Hori, C.E. Effect of different promoters on $Ni/CeZrO_2$ catalyst for autothermal reforming and partial oxidation of methane. *Chem. Eng. J.* **2010**, *156*, 380–387. [CrossRef]
22. Escritori, J.C.; Dantas, S.C.; Soares, R.R.; Hori, C.E. Methane autothermal reforming on nickel–ceria–zirconia based catalysts. *Catal. Commun.* **2009**, *10*, 1090–1094. [CrossRef]
23. Ismagilov, I.Z.; Matus, E.V.; Kuznetsov, V.V.; Kerzhentsev, M.A.; Yashnik, S.A.; Prosvirin, I.P.; Mota, N.; Navarro, R.M.; Fierro, J.L.G.; Ismagilov, Z.R. Hydrogen production by autothermal reforming of methane over NiPd catalysts: Effect of support composition and preparation mode. *Int. J. Hydrog. Energy* **2014**, *39*, 20992–21006. [CrossRef]
24. Lim, S.-S.; Lee, H.-J.; Moon, D.-J.; Kim, J.-H.; Park, N.-C.; Shin, J.-S.; Kim, Y.-C. Autothermal reforming of propane over Ce modified Ni/LaAlO3 perovskite-type catalysts. *Chem. Eng. J.* **2009**, *152*, 220–226. [CrossRef]
25. Lee, H.-J.; Lim, Y.-S.; Park, N.-C.; Kim, Y.-C. Catalytic autothermal reforming of propane over the noble metal-doped hydrotalcite-type catalysts. *Chem. Eng. J.* **2009**, *146*, 295–301. [CrossRef]
26. Choudhary, V.R.; Rane, V.H.; Rajput, A.M. Simultaneous thermal cracking and oxidation of propane to propylene and ethylene. *AIChE J.* **1998**, *44*, 2293–2301. [CrossRef]
27. Frontera, P.; Antonucci, P.L.; Macario, A. Focus on Materials for Sulfur-Resistant Catalysts in the Reforming of Biofuels. *Catalysts* **2021**, *11*, 1029. [CrossRef]
28. Lo Faro, M.; Antonucci, V.; Antonucci, P.L.; Aricò, A.S. Fuel flexibility: A key challenge for SOFC technology. *Fuel* **2012**, *102*, 554–559. [CrossRef]
29. Ruiz, J.A.C.; Passos, F.B.; Bueno, J.M.C.; Souza-Aguiar, E.F.; Mattos, L.V.; Noronha, F.B. Syngas production by autothermal reforming of methane on supported platinum catalysts. *Appl. Catal. A Gen.* **2008**, *334*, 259–267. [CrossRef]
30. Pino, L.; Vita, A.; Cipitì, F.; Lagana, M.; Recupero, V. Performance of Pt/CeO_2 catalyst for propane oxidative steam reforming. *Appl. Catal. A Gen.* **2006**, *306*, 68–77. [CrossRef]
31. Feret, F.R. Determination of the crystallinity of calcined and graphitic cokes by X-ray diffraction. *Analyst* **1998**, *123*, 595–600. [CrossRef]
32. Menon, P.G. Coke on catalysts-harmful, harmless, invisible and beneficial types. *J. Mol. Catal.* **1990**, *59*, 207–220. [CrossRef]
33. Argyle, M.D.; Bartholomew, C.H. Heterogeneous Catalyst Deactivation and Regeneration: A Review. *Catalysts* **2015**, *5*, 145–269. [CrossRef]